IMPACT OF FEEDSTOCK TYPE AND PYROLYSIS TEMPERATURE ON BIOCHAR PROPERTIES AND SOIL PHYSIOCHEMICAL CHARACTERISTICS IN El-HAMMAM REGION, EGYPT

Sahar M. Ismail
Department of Soil Chemistry and Physics, Water Resources and Desert Soils Division, Desert Research Center, Cairo, Egypt
E-mail: dr.sahar.mohamedi@gmail.com

Biochar has emerged as a sustainable soil amendment for improving soil quality in arid and semi-arid regions with low fertility and organic matter content. This study evaluated the effects of biochars produced from olive pomace (PO), goat-sheep dung (GSD) and poultry manure (PM), pyrolyzed at 350, 500 and 700°C, on the physiochemical properties of degraded sandy soil in the El-Hammam region, Egypt. Characterization of feedstocks and biochars was conducted using proximate, ultimate, thermogravimetric and differential thermal analyses (TGA-DTA), Fourier Transform Infrared (FT-IR), Brunauer–Emmett–Teller (BET) surface area analysis, Scanning Electron Microscopy (SEM), X-ray Diffraction (XRD) and X-ray Fluorescence (XRF). Based on structural stability, surface area and nutrient content, biochars produced at 500°C were selected for greenhouse pot experiments. Each biochar type was applied at 2 and 5% (w w^{-1}) to sandy soil for a 60-day incubation period. Biochar properties, including pH, EC, ash content, elemental composition and density, were analyzed. Post-incubation, soil properties such as pH, EC, total organic carbon (TOC), total nitrogen (TN), C/N ratio, cation exchange capacity (CEC), porosity, and available water content (AWC) were assessed. Results showed that both feedstock type and pyrolysis temperature significantly affected biochar characteristics and soil responses. PO biochar at 5% and 500°C showed the highest increases in TOC (50%), porosity (47.92) and AWC (14.2%). PM biochar achieved the highest CEC (85 cmol kg^{-1}), while GSD biochar provided moderate improvements. PO biochar at 500°C and 5% application is recommended as the most effective application for enhancing soil fertility and water retention under arid conditions.

Keywords: olive pomace, poultry manure, goat and sheep dung, sandy loam, soil physiochemical properties, El-Hammam region

INTRODUCTION

The El-Hammam region in northwestern Egypt, characterized by extensive agricultural and pastoral activities, faces growing environmental and agronomic challenges due to the accumulation of organic waste. The intensification of olive oil production, widespread small ruminant farming, and rapid expansion of the poultry industry have generated significant quantities of biomass residues-primarily olive pomace (PO), sheep and goat dung, and poultry manure (El-Shafie et al., 2022). In the absence of effective waste management systems, these materials are often disposed of through open dumping or uncontrolled combustion, resulting in environmental degradation, including soil and water contamination, air pollution, greenhouse gas emissions and public health risks (Ahmed et al., 2019; Kumar et al., 2020 and Youssef et al., 2023). Biochar production through pyrolysis offers a sustainable pathway for managing these residues. Pyrolysis—thermal decomposition of biomass under limited oxygen—produces biochar, a stable, carbon-rich material with high porosity, surface area and aromaticity. These properties enhance biochar's ability to improve soil fertility, increase water retention, sequester carbon and adsorb environmental pollutants (Lehmann et al., 2011 and Lehmann and Joseph, 2015). Such functions are particularly relevant to arid and semi-arid zones like El-Hammam, where soils typically suffer from low organic matter, salinity and poor water-holding capacity (Jeffery et al., 2017; Abdel-Rahman et al., 2022 and El-Beltagy et al., 2023). Biochar characteristics are highly dependent on both the biomass feedstock and pyrolysis conditions including temperature, heating rate and residence time (Wang et al., 2020). Thus, tailoring biochar properties to meet specific environmental or agronomic goals requires a detailed understanding of these interactions. In El-Hammam, the selected feedstocks-olive pomace, sheep and goat dung and poultry manure; are abundant and chemically diverse, each conferring unique properties to the resulting biochar. Olive pomace, a lignocellulosic residue from olive oil extraction, is rich in cellulose, hemicellulose and lignin. Its biochar is typically high in fixed carbon (FC), structurally aromatic and thermally stable, with enhanced porosity and surface reactivity for nutrient and water retention and pollutant adsorption (Smith et al., 2018 and Hassan et al., 2021). Studies have demonstrated its efficacy in improving soil structure, nutrient cycling and reducing agrochemical leaching (Al-Wabel et al., 2019).

Sheep and goat dung, enriched with nitrogen and minerals due to extensive pastoralism in the region, produces nutrient-rich biochar that can stimulate soil microbial communities, enhance nitrogen cycling and improve soil texture (Rajkovich et al., 2012 and Zama et al., 2020). However, its high nutrient content can result in elevated ash levels and the potential release of trace metals during pyrolysis, necessitating controlled processing for safety and effectiveness. Poultry manure is especially high in macronutrients (N, P,

K), making its biochar a promising soil amendment. When optimized, poultry manure biochar can enhance soil fertility, reduce nitrogen leaching, and support microbial activity (Xu et al., 2020 and Chen et al., 2021).

Nevertheless, its high ash content and low FC may limit long-term stability and require careful pyrolysis optimization to enhance nutrient retention and minimize risks such as heavy metal contamination or ammonia volatilization. Pyrolysis temperature is a critical factor affecting biochar quality. Low-temperature pyrolysis (300-500°C) retains more labile organic matter and nutrients, favoring short-term soil fertility improvements. In contrast, high-temperature pyrolysis (>600°C) enhances aromatic carbon content, surface area and structural stability, improving long-term carbon sequestration and pollutant adsorption (Wang et al., 2020). Optimizing temperature is thus essential for aligning biochar performance with intended applications. To comprehensively characterize and optimize biochar production, Thermogravimetric Analysis (TGA) offers essential insights into the thermal behavior of biomass feedstocks. TGA measures the mass loss of a sample as a function of temperature under controlled conditions, thereby revealing its thermal decomposition profile, including the sequential release of moisture, volatile matter and the formation of FC. By analyzing these transitions, TGA facilitates the precise calibration of pyrolysis conditions; such as temperature thresholds and residence times, ensuring consistent biochar quality and stability across different feedstocks (Basu, 2013 and Ahmad et al., 2014). In the absence of TGA, the natural variability in feedstock composition could lead to suboptimal or inconsistent pyrolysis outcomes, ultimately compromising the agronomic or environmental performance of the resulting biochar.

In parallel with (TGA), Differential Thermal Analysis (DTA) provides valuable complementary insights into the thermal behavior of biochar feedstocks. DTA measures the temperature difference between a sample and an inert reference material during controlled heating, thereby identifying endothermic and exothermic processes associated with key thermal transitions; such as moisture evaporation, decomposition of organic constituents (hemicellulose, cellulose and lignin) and mineral transformations (Méndez et al., 2013 and Inyang et al., 2016). These thermal processes are critical for understanding the reactivity and energy dynamics of the feedstock during pyrolysis. When interpreted alongside TGA data, DTA facilitates the correlation of mass loss with specific thermal reactions, enabling precise adjustment of pyrolysis parameters to optimize desirable biochar characteristics, such as carbon stability, porosity and nutrient retention. Additionally, DTA enables the identification of thermal stability thresholds and oxidation peaks, contributing to the development of safe and efficient biochar production strategies (Antal and Grønli, 2003).

This integrated thermal analysis approach enhances the understanding of feedstock-specific behavior and supports the targeted optimization of pyrolysis conditions, particularly in environmentally sensitive and agronomically challenged regions such as El-Hammam. Despite global advances in biochar research, localized studies in El-Hammam are lacking. Considering the region's unique soil types, climatic conditions, and agricultural practices, conducting location-specific studies is crucial to evaluate the effectiveness of biochar in enhancing soil quality and boosting agricultural productivity (El-Gohary et al., 2023). Moreover, the successful adoption of biochar technologies depends not only on agronomic performance but also on economic feasibility, farmer acceptance and institutional support (FAO, 2021). By converting local organic residues through biochar production, El-Hammam region has the opportunity to advance sustainable agriculture, improve soil health and mitigate environmental harm. This approach supports circular bioeconomy principles by enhancing resource efficiency, closing nutrient loops and promoting climate resilience.

This study aims to: (1) Produce and characterize biochars from olive pomace, sheep and goat dung and poultry manure using pyrolysis at 350, 500 and 700°C, (2) Select an optimal pyrolysis temperature based on biochar physicochemical properties and prepare biochars at this temperature for soil application, (3) Assess the effects of biochar application (at 2 and 5% w w^{-1}) on the physiochemical properties of El-Hammam soils in a controlled pot experiment simulating field conditions, (4) Compare the performance of different feedstock-derived biochars at the selected pyrolysis temperature to determine the most effective combination of feedstock and application rate for improving soil quality in arid and semi-arid environments.

MATERIALS AND METHODS

1. Study Area Description

The study was conducted in El-Hammam, situated along the northwestern Mediterranean coast of Egypt, west of Alexandria, between latitudes 30°40′–30°55′ N and longitudes 29°10′–29°30′ E. This region falls within an arid to semi-arid Mediterranean climatic zone, characterized by hot, dry summers and mild winters. Annual precipitation typically ranges between 100 and 150 mm (Mahmoud et al., 2009). The study area is characterized by flat to gently undulating topography with shallow depressions and scattered sand dunes, at elevations ranging from 10 to 50 meters above sea level. The soils, mainly sandy loam to loamy sand with low clay and organic matter, are weakly structured and exhibit poor water retention and fertility (Shendi et al., 2024). Salinization, driven by shallow groundwater and high evaporation, poses a major challenge, particularly in reclaimed lands, reducing productivity and accelerating degradation (Mahmoud and Abd-Elrahman, 2025). Sparse

native halophytic vegetation helps stabilize the soil and supports ecological resilience under these harsh conditions.

2. Feedstock Collection and Pre-treatment

Three types of agricultural residues were selected as feedstocks: olive pomace (sourced from olive oil extraction), poultry manure (collected from poultry farms) and a 1:1 mixture of goat and sheep dung (gathered from multiple locations). All materials were obtained from local agricultural and livestock sources within the El-Hammam region. Following collection, the feedstocks were immediately transported to the laboratory in airtight containers to prevent moisture uptake, oxidation and external contamination. Each residue type was first air-dried at ambient room temperature (~25°C) for 48 hours, then oven-dried at 100°C for 24 hours to remove any residual moisture (Ahmad et al., 2014). The dried samples were subsequently ground using a mechanical grinder and sieved to a particle size of ≤2 mm with a mechanical sieve shaker to ensure homogeneity for subsequent pyrolysis and analytical procedures.

3. Pyrolysis Procedure

Biochar was produced from each of the three feedstocks; olive pomace, poultry manure and the goat-sheep dung mixture; using a lab-scale fixed-bed tubular pyrolysis reactor (Model: Nabertherm LHT 02/17 LB, Germany) under oxygen-limited conditions (Fig. 1). Pyrolysis for each feedstock was conducted in triplicate to ensure reproducibility. Approximately 50 g of pre-treated biomass was placed in a quartz reactor, purged with ultra-high purity nitrogen at 100 mL min^{-1} for 30 minutes to remove oxygen, with the inert nitrogen atmosphere maintained throughout the process to prevent oxidation (Gupta et al., 2019). The reactor was then heated at a constant rate of 10 °C min^{-1} to target final temperatures of 350, 500 and 700°C. At each peak temperature, the system was held isothermally for 30 minutes to allow complete carbonization and stabilization of the resulting biochar (Ahmad et al., 2014). After pyrolysis, the reactor was allowed to cool naturally to ambient room temperature under continuous nitrogen flow to prevent post-pyrolysis oxidation. Once cooled, the resulting biochar was carefully collected, weighed to calculate pyrolysis yield and stored in airtight polyethylene containers to protect it from moisture absorption and external contamination prior to subsequent physiochemical analyses.

4. Biochar Analytical Procedures

4.1. Characterization of raw feedstock materials

Moisture content was determined by oven-drying at 105°C for 24 hours following the AOAC (2000) guidelines. Ash content and volatile matter were measured according to ASTM E1755-01 and ASTM E872-82 protocols, respectively (ASTM, 2019 and ASTM, 2020). Fixed carbon (FC) content was calculated by difference as per Basu (2013):

$$FC = 100 - M - VM - Ash\ (\%)$$

Where, M is moisture content (%) and VM is volatile matter (%).

Elemental composition (C, H, N, S) was quantified using a LECO CHNS analyzer according to ASTM D5373-14 and ASTM D4239-12 standards (ASTM, 2018 and ASTM, 2021). Oxygen (O) content was not measured directly but calculated by difference from the total using the equation:

$$O\ (\%) = 100 - (C + H + N + S + Ash)$$

Thermal stability and decomposition behavior were assessed using (TGA) with a Perkin Elmer STA 6000. Dry samples were heated from ambient temperature to 950°C at a rate 10°C min^{-1} under a nitrogen flow to characterize sequential thermal degradation stages, as described by Méndez et al. (2013) and Carrier et al. (2011).

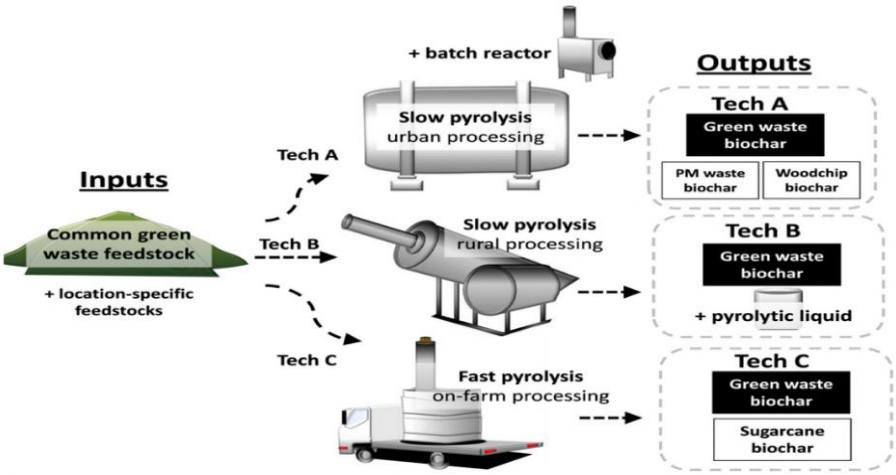

Fig. (1). Schematic diagram of the lab-scale fixed-bed tubular pyrolysis reactor (Nabertherm LHT 02/17 LB, Germany) used in this study for the thermal conversion of agricultural residues into biochar under oxygen-limited conditions.

4.2. Physicochemical characterization of biochar samples

Following pyrolysis at target temperatures of 350, 500 and 700°C, the resulting biochar samples were subjected to comprehensive physicochemical characterization to evaluate their structural, chemical and functional properties. Fourier Transform Infrared Spectroscopy (FT-IR) was conducted using a PerkinElmer Spectrum BX spectrometer across a wavenumber range of 4000–650 cm^{-1} to identify surface functional groups and assess the chemical structure and stability of the biochars. Nitrogen adsorption–desorption isotherms at 77 K were employed to determine surface area and pore structure using the Brunauer–Emmett–Teller (BET) method. Prior to

analysis, all samples were degassed at 250°C for 4 hours to remove adsorbed gases and moisture (Lowell et al., 2014).

Scanning Electron Microscopy (SEM) was used to examine surface morphology and pore development. Crystalline mineral phases were identified by X-ray Diffraction (XRD) using a GBC-EMMA diffractometer. Macro- and micronutrient content, as well as potential heavy metals, were determined using X-ray Fluorescence (XRF; Elvatech system). Cation Exchange Capacity (CEC) was determined using the ammonium acetate saturation method at pH 7.0, as outlined by Sumner and Miller (1996), and results were reported in cmol kg^{-1}. Total Organic Carbon (TOC) was quantified using the wet oxidation method with potassium dichromate and sulfuric acid, following Nelson and Sommers (1996). Total Nitrogen (TN) was determined using the Kjeldahl method, involving acid digestion, distillation and titration, following the procedures outlined by Nelson and Sommers (1996). TOC and TN were analyzed for both the feedstocks and the corresponding biochars. The C/N ratio was subsequently calculated to assess biochar stability and potential agronomic effectiveness. pH and Electrical Conductivity (EC) were measured in a 1:10 (w/v) biochar-to-deionized water suspension using a calibrated pH meter and conductivity meter, respectively, according to Sparks (1996). Density was determined using the tapping method, whereby biochar was loaded into a graduated cylinder and tapped until the volume stabilized, as per Chen et al. (2012).

The biochar yield (%) was calculated as the ratio of the dry weight of the produced biochar to the dry weight of the original feedstock, serving as an indicator of pyrolysis efficiency.

Biochar Yield (%) =

[Weight of biochar after pyrolysis /Initial dry weight of feedstock]× 100

All measurements were performed in triplicate and results are presented as mean values ± standard deviation to ensure accuracy and statistical reliability.

5. Selection of Optimal Pyrolysis Temperature and Biochar Production

Based on the physicochemical characterization results presented later, a pyrolysis temperature of 500°C was selected as the optimal condition for producing biochar from olive pomace (PO), poultry manure (PM) and goat-sheep dung (GSD). This temperature was chosen due to its favorable balance between high carbon content, moderate biochar yield, structural stability and significant transformation of surface functional groups, as indicated by FT-IR and elemental analysis. Biochars from all three feedstocks were produced following a standardized slow pyrolysis procedure under oxygen-limited conditions in a laboratory-scale muffle furnace. The process employed a heating rate of 10°C per minute, with a residence time of 30 minutes at the target temperature, followed by natural cooling within the furnace. The obtained biochars were then ground to pass through a 2 mm sieve, thoroughly

homogenized and stored in airtight containers to preserve their properties for subsequent soil application and analysis (Gupta et al., 2019).

6. Pot Experiment to Evaluate Biochar Effects on Soil Physiochemical Properties

A greenhouse pot experiment was conducted to evaluate the effects of biochar application on the physiochemical properties of El-Hammam soil, representative of arid and semi-arid regions. Surface soil samples (0-30 cm depth) were collected from the El-Hammam region, air-dried and sieved through a 2 mm mesh. The experimental design included three biochar types PO, PM and GSD; applied at two application rates (2 and 5% w w^{-1}), along with a control treatment without biochar. Each treatment was replicated three times. For each replicate, 3 kg of dry soil was thoroughly mixed with the designated amount of biochar and placed in plastic pots. Moisture levels were maintained at 60% of the soil's water holding capacity (WHC), determined gravimetrically according to the method of Klute (1986). The pots were incubated under controlled greenhouse conditions at 25 ± 2°C with a relative humidity of 60-70% for 60 days. At the end of the incubation period, soil samples were collected and analyzed for several physiochemical parameters. Soil pH was measured in a 1:2.5 soil-to-water suspension using a Hanna Instruments HI 2211 pH meter (Thomas, 1996) and EC was determined in the same extract using a Hanna Instruments HI 993310 EC meter (Rhoades, 1996). TOC was analyzed using the Walkley–Black dichromate oxidation method (Nelson and Sommers, 1996), while total organic nitrogen (TON) was quantified by the Kjeldahl digestion method (Bremner and Mulvaney, 1982). The carbon-to-nitrogen (C/N) ratio was calculated based on TOC and TON values. CEC was determined using the ammonium acetate extraction method at pH 7.0 (Sumner and Miller, 1996). Bulk density was determined using the core method as described by Blake and Hartge (1986). In addition, the water holding capacity was reassessed after incubation to evaluate the changes induced by biochar application, following the gravimetric method described by Klute (1986). Soil porosity was estimated using bulk density and an assumed particle density of 2.65 g cm^{-3}.

Water retention was assessed by gravimetrically determining the soil moisture content at available water content at field capacity (AWC_fc) and permanent wilting point (PWP), using the pressure plate apparatus in accordance with Reynolds et al. (2002). Soil samples were first saturated and then subjected to matric potentials of −33 kPa to determine AWC_fc and −1500 kPa for PWP. After reaching equilibrium at each pressure level, the samples were allowed to drain and subsequently oven-dried at 105°C for 24 hours. The gravimetric moisture content (θg) at each pressure point was calculated using the following equation:

$$\theta g\ (\%) = [(W_{wet} - W_{dry}) / W_{dry}] \times 100$$

Where, W_{wet} is the weight of moist soil at either field capacity or wilting point; and W_{dry} is the weight of the oven-dry soil. The available water content (AWC) was then calculated as the difference between AWC_fc and PWP:

$$AWC = \theta_{AWC\_fc} - \theta_{PWP}$$

All measurements were carried out in triplicate. Statistical analysis was performed using a one-way analysis of variance, followed by Tukey's Honest Significant Difference (HSD) post hoc test to determine statistically significant differences among treatment means at a significance level of $p < 0.05$. The analysis was conducted using IBM SPSS Statistics for Windows, version 25 (IBM Corp., 2017).

RESULTS AND DISCUSION

1. Feedstock and Derived Biochar Characterization

1.1. Proximate analysis

The physicochemical characterization of PM, GSD and PO provides critical insights into their suitability for thermochemical conversion and biochar production. The proximate analysis results, presented in Table (1), reveal significant variations among the three feedstocks in terms of organic matter (OM), volatile matter (VM), ash content and FC. Biochar produced from PM exhibited the highest OM (73.36%$_{dw}$) and VM (69.21%$_{dw}$) contents, reflecting a high proportion of thermally labile organic compounds. These values are consistent with findings from Quiroga et al. (2010), Cely et al. (2015) and Hu et al. (2022), who reported OM and VM ranges of 62.8–71.5% and 42.4–69.51%, respectively. However, the high ash content of PM biochar (28.60%$_{dw}$), though within the reported range of 14.66-53.2%, may adversely affect pyrolysis efficiency by reducing energy density and influencing reaction pathways due to the catalytic activity of mineral constituents (Tripathi et al., 2016 and Munawar et al., 2021).

Additionally, the relatively low FC content (4.15%$_{dw}$) indicates limited thermal recalcitrance, likely resulting from microbial degradation during storage, the inclusion of bedding materials, or variability in manure composition (Cely et al., 2015 and Awasthi, 2020). In comparison, GSD biochar exhibited lower OM (55.35%$_{dw}$) and VM (52.45%$_{dw}$) contents compared to PM and PO but still falls within the expected range for ruminant-derived feedstocks. The reduced values may be attributed to microbial decomposition or prolonged storage, as suggested by Otero et al. (2002). GSD also had a relatively high ash content (22.44%$_{dw}$), indicating a substantial mineral fraction, which can hinder pyrolysis efficiency and reduce biochar yield. Furthermore, GSD recorded the lowest FC content among the three feedstocks, as previously noted by Awasthi et al. (2020). In contrast, PO showed a more favorable composition for biochar production. It's high OM (69.00%$_{dw}$) and VM (64.50%$_{dw}$) contents suggest strong energy potential and thermal reactivity.

Table (1). The results of proximate analysis for feedstocks.

Sample code	Sample type	Organic matter content ($\%_{dw}$)	Volatile matter ($\%_{dw}$)	Ash ($\%_{dw}$)	Fixed carbon ($\%_{dw}$)
GSD	Goat-sheep dung	55.35	52.45	22.44	2.90
PM	Poultry Manure	73.36	69.21	28.60	4.15
PO	Olive Pomace	69.00	64.50	7.42*	4.50
—	Literature range **	62.8-71.5	42.4-69.51	14.66-53.2	1.8-20.67

*Slightly lower than common range, possibly due to removal of pits and mineral-free processing. Still within acceptable range reported by Domingues et al. (2017). ** References: Otero, et al., 2002; Thipkhunthod, et al., 2005; Quiroga et al., 2010 and Cely, et al., 2015

Notably, PO exhibited the lowest ash content (7.42%$_{dw}$), even slightly lower than values reported by Domingues et al. (2017), likely due to effective removal of pits and other inorganic impurities during processing. The low ash content is beneficial for enhancing thermal conversion efficiency, minimizing fouling or slagging risks and improving energy recovery during pyrolysis (Munawar et al., 2021). Additionally, the moderate FC content (4.50%$_{dw}$) reflects a balanced carbon structure suitable for both energy release and stable char formation. Several studies have confirmed that biochar derived from PO typically possesses favorable surface area, porosity, and adsorption capacity, along with enhanced soil conditioning properties (Cely et al., 2015 and Domingues et al., 2017).

1.2. Ultimate analysis

PO exhibited the highest carbon content (40.65%$_{dw}$) (Table 2), suggesting a strong lignocellulosic composition with elevated levels of cellulose and lignin. This structure is conducive to the production of stable, carbon-rich biochar with high energy density and surface reactivity (Ahmad et al., 2014 and Domingues et al., 2017). Additionally, PO showed the highest oxygen content (43.62%$_{dw}$), indicating a significant presence of oxygenated functional groups (like hydroxyl, carbonyl and carboxyl). These groups are precursors to valuable volatiles; such as furans, alcohols and organic acids, formed during pyrolysis (Cely et al., 2015 and Otero et al., 2002). Notably, PO contained the lowest nitrogen (1.90%$_{dw}$) and sulfur (0.30%$_{dw}$) levels, minimizing the risk of NO_x and SO_x emissions. Consequently, PO emerges as the most promising candidate among the studied feedstocks for low-emission, high-yield biochar and bioenergy applications. In contrast, PM exhibited the highest nitrogen content (5.52%$_{dw}$), which aligns with its rich composition of proteins, urea, and uric acid (Thipkhunthod et al., 2005). While this elevated nitrogen content supports the production of nutrient-enriched biochar, beneficial for improving soil fertility, it may also increase NO_x emissions during thermal treatment. PM showed moderate carbon (34.70%$_{dw}$) and hydrogen (5.42%$_{dw}$) levels, slightly lower than those of PO, reflecting a somewhat lower energy potential. GSD displayed intermediate elemental properties, with carbon at

39.82%$_{dw}$, hydrogen at 5.20%$_{dw}$ and nitrogen at 4.12%$_{dw}$, values that are consistent with literature reports on ruminant manures (Otero et al., 2002 and Cely et al., 2015).

Table (2). The results of ultimate analysis for feedstocks.

Sample code	C (%$_{dw}$)	H (%$_{dw}$)	N (%$_{dw}$)	S (%$_{dw}$)	*O (%$_{dw}$)
GSD	39.82	5.20	4.12	0.5	27.92
PM	34.70	5.42	5.52	0.6	25.16
PO	40.65	6.11	1.90	0.3	43.62
Literature range **	21.21-41.13	3.35-5.89	2.69-5.9	0.11-1.03	20.75-49.92

*Oxygen content was calculated by difference: O% = 100 - (C + H + N + S + Ash)
** References: Otero et al. (2002), Thipkhunthod et al. (2005), Quiroga et al. (2010) and Cely et al. (2015).

1.3. Thermal behavior based on TGA-DTA and proximate/ultimate analysis

Fig. (2) shows TGA and DTA of PO, PM and GSD. In all three feedstocks, the principal mass loss occurred between 200 and 500°C, corresponding to the decomposition of hemicellulose, cellulose and the early stages of lignin degradation. A minor endothermic peak near 100°C appeared in each DTA curve, attributed to the evaporation of moisture. This was followed by a prominent exothermic peak around 280-300°C, indicative of the combustion of volatile organic compounds.

Among the samples, PO exhibited the highest thermal stability, reflected by its lower total mass loss and greater char yield in the TGA curve. This behavior corresponds with its high carbon content (40.65%), low ash content (7.42%) and moderate volatile matter (64.50%), as shown in Tables (1) and (2).

The relatively high oxygen content (43.62%) and lignocellulosic composition further contribute to a gradual thermal degradation, as confirmed by the broad and less intense exothermic peak in the DTA curve. These results align with the findings of García-Maraver et al. (2010), who reported that olive pomace undergoes de-volatilization primarily between 200-450°C and forms stable char around 600-700°C. Conversely, PM displayed the fastest decomposition rate, with the highest mass loss and lowest residual mass, likely due to its high volatile matter (69.21%), elevated ash content (28.60%) and lowest carbon content (34.70%). These characteristics promote rapid de-volatilization and reduced char formation. The DTA curve showed strong exothermic activity around 300°C, consistent with the decomposition of nitrogen-rich and proteinaceous materials common in poultry waste. Two distinct stabilization plateaus observed in the PM, TGA curve; around 450 and 600°C, suggest sequential stages of char formation. This behavior is supported by Gao et al. (2020), who reported similar decomposition behavior and

exothermic profiles in poultry manure. GSD exhibited intermediate thermal behavior, with a moderate mass loss rate and final char residue. The TGA curve showed stabilization zones near 660 and 750°C, indicative of progressive char formation and thermal resistance. This aligns with GSD's balanced composition; moderate volatile matter (52.45%), ash (22.44%) and relatively high carbon content (39.82%), as well as its presumed higher lignin content, which decomposes at higher temperatures. These observations are corroborated by Cantrell et al. (2012), who found goat and sheep manure exhibited major decomposition between 200-500°C and char development extending up to 750°C.

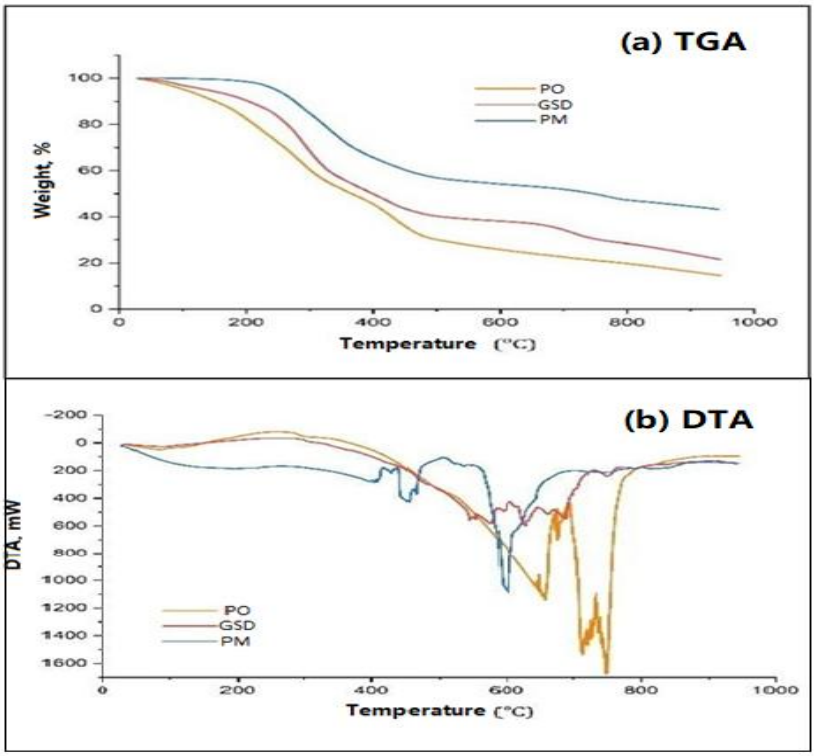

Fig. (2). Thermogravimetric (TGA) and Differential Thermal Analyses (DTA) profiles of Olive Pomace (PO), Poultry Manure (PM), and Goat-Sheep Dung (GSD), **a.** TGA curves illustrating mass loss patterns with increasing temperature, **b.** DTA curves showing endothermic and exothermic processes during decomposition.

1.4. Biochar yield of waste samples

The yield of biochar decreased consistently with increasing pyrolysis temperature across all three feedstocks (Table 3), in accordance with established thermal decomposition behavior reported by Ahmad et al. (2014) and Hassan et al. (2020). This inverse relationship reflects the progressive

volatilization of organic matter and the thermal degradation of carbonaceous compounds at elevated temperatures (Wang et al., 2020). Among the three residues, PO produced the highest biochar yields at all temperatures; 63.64% at 350°C, 52.74% at 500°C and 37.79% at 700°C. This high yield corresponds with PO's low ash content (7.42%) and high carbon (40.65%) and oxygen (43.62%) levels, which favor the formation of thermally stable, aromatic structures. The results are consistent with Domingues et al. (2017), who reported similar yields and stability profiles for olive-derived biochars. In contrast, GSD exhibited the lowest biochar yields; 52.07% at 350°C decreasing to 22.56% at 700 °C. This low performance is attributable to its low FC content (2.90%) and high ash content (22.44%), which limit biochar formation and enhance mineral volatilization. These observations are in agreement with previous studies by Cely et al. (2015) and Zama et al. (2020), who found that high-ash manure feedstocks typically yield less biochar under similar pyrolytic conditions. PM demonstrated moderate and relatively stable biochar yields across the temperature range, with a peak yield of 39.33% at 500°C. This performance is likely due to its high organic matter (73.36%) and volatile matter (69.21%) contents, which enhance char formation at moderate temperatures. Despite its high ash content (28.60%), the nitrogen-rich composition of PM may contribute to the early stabilization of char structures, as supported by findings from Gao et al. (2020). Overall, while lower pyrolysis temperatures (350-500°C) promote higher biochar yields, they may compromise biochar stability. Conversely, higher temperatures (700°C) produce biochars with enhanced aromaticity and resistance to microbial degradation, which are essential for long-term carbon sequestration and pollutant immobilization (Lehmann and Joseph, 2015).

Table (3). Biochar yield (%) of different feedstocks at varying pyrolysis temperatures.

Feedstock	**Biochar yield (%)**		
Temperature (°C)	**350**	**500**	**700**
GSD	52.07 (±1.25)	30.09 (±0.84)	22.56 (±0.65)
PM	52.49 (±1.12)	39.33 (±0.90)	35.48 (±0.78)
PO	63.64 (±1.40)	52.74 (±1.10)	37.79 (±0.95)

Note: Values in parentheses indicate standard deviation (n = 3).

1.5. Fourier Transform Infrared (FT-IR) spectroscopy

Fig. (3) shows the FT-IR spectroscopy of GSD, PM and PO at pyrolysis temperatures of 350, 500 and 700°C. A broad and intense absorption band between 3304-3280 cm^{-1}, corresponding to O–H stretching vibrations from hydroxyl groups and adsorbed water, was distinctly present in the raw feedstocks (Chen et al., 2016). This band disappeared after pyrolysis at 350°C across all feedstocks, particularly in PO. This is consistent with moisture loss and thermal dehydration processes, supported

by TGA mass loss profiles (Fig. 2a) and previous literature by Chen et al. (2017) and Wu et al. (2021), which report that hydroxyl groups decompose at temperatures between 300-400°C.

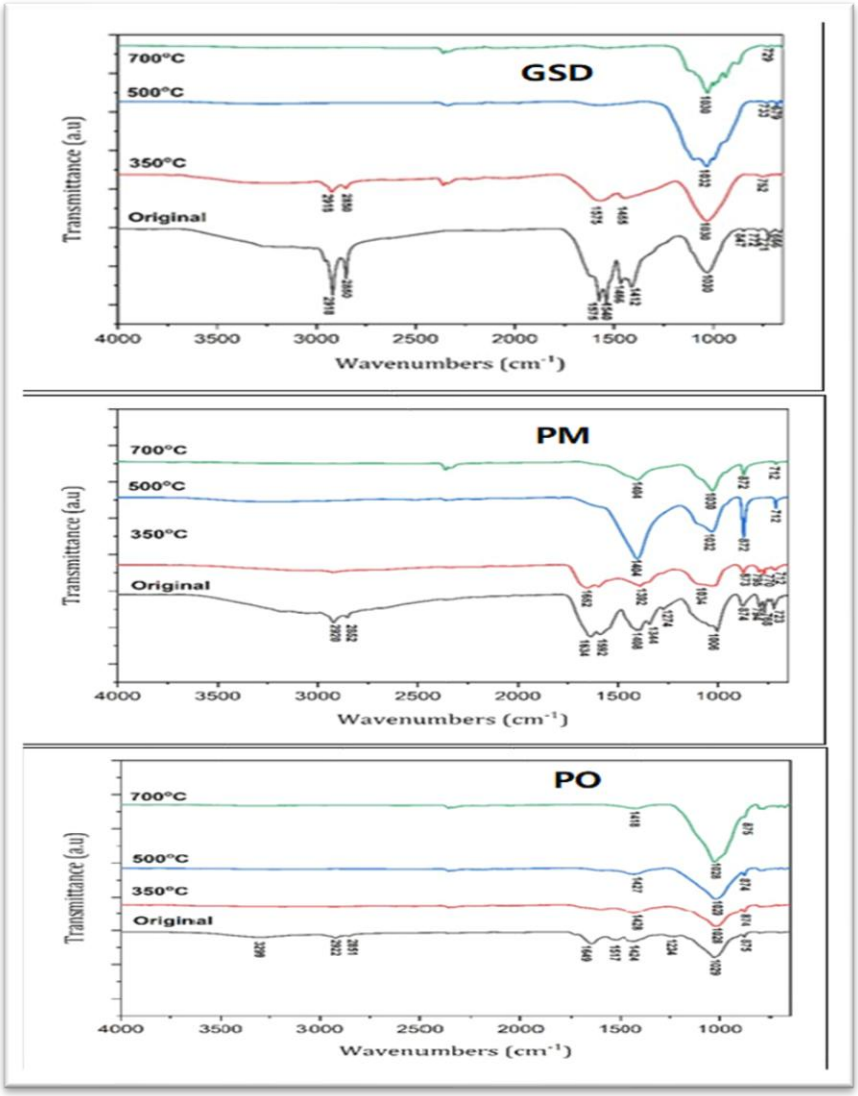

Fig. (3). FT-IR spectra of raw feedstocks and their biochars produced at 350, 500 and 700°C, showing the evolution and loss of surface functional groups (O–H, C–H, C=O and C–O) with increasing pyrolysis temperature.

Additionally, the progressive weakening of the C–O stretching bands in the 1274-1014 cm^{-1} region; associated with cellulose and hemicellulose polysaccharides, was observed with increasing pyrolysis

temperature, which is consistent with the findings of Sun et al. (2012). This transformation was especially prominent in PO and PM, indicating extensive decomposition of carbohydrate structures. These findings correlate well with the decrease in volatile matter and corresponding increase in FC (Table 1), along with reduced oxygen content (Table 2). This degradation process supports the transition toward condensed aromatic structures, as reported by Domingues et al. (2017) and Zhang et al. (2020). At 700°C, new bands appeared in the 877-666 cm^{-1} region, attributed to aromatic C–H out-of-plane bending vibrations, confirming the formation of polyaromatic and graphitic domains. These bands were most prominent in PO-derived biochar, indicating the development of thermally stable carbon structures (Song and Guo, 2012 and Siengchum et al., 2013). This aromatic development is consistent with the high FC content of PO (Table 1), elevated C content (Table 2) and its lower biochar yield at higher temperatures (Table 3), all indicating advanced carbonization.

Furthermore, the FT-IR results correspond well with the BET surface area data (Table 4 and Fig. 4). PO biochar showed strong attenuation of polar functional groups even at 350-500°C, which matches the increase in surface area at 500°C (41.76 $m^2\ g^{-1}$), before a drop at 700°C. This suggests structural reordering or pore collapse at high temperature; a conclusion supported by SEM analysis and studies by Singh et al. (2022). In contrast, GSD biochar showed progressive transformation and a more linear surface area increase, aligning with the smoother loss of FT-IR bands and thermal decomposition stages shown in TGA-DTA.

Table (4). BET surface area and pore volume of biochars derived from GSD, PM and PO at different pyrolysis temperatures.

Sample code	BET surface area ($m^2 g^{-1}$)	Pore volume ($cm^3 g^{-1}$)
GSD-350	1.6296	0.008
GSD-500	22.9497	0.138
GSD-700	47.5858	0.357
PM-350	7.8414	0.055
PM-500	9.7394	0.061
PM-700	11.3092	0.606
PO-350	1.9192	0.287
PO-500	41.7567	0.024
PO-700	21.2004	1.002

Note: GSD = Goat-Sheep Dung, PM = Poultry Manure, PO = Olive Pomace

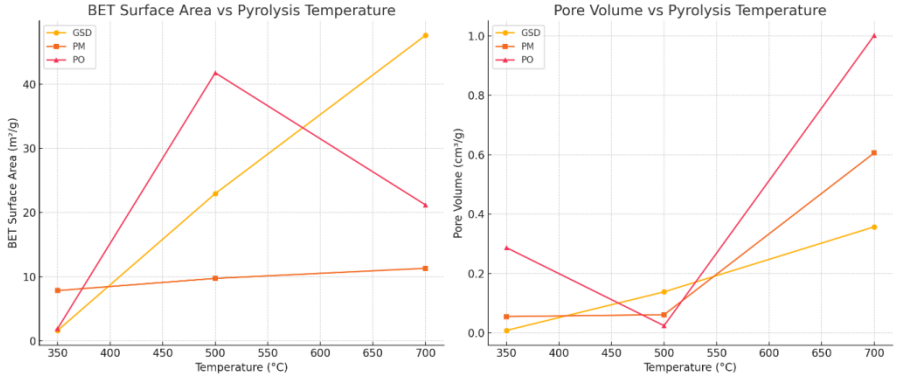

Fig. (4). Effect of pyrolysis temperature on BET surface area and pore volume of biochars derived from GSD, PM and PO.

1.6. Brunauer–Emmett–Teller (BET) surface area and pore volume analysis

The BET surface area and pore volume of biochars derived from GSD, PM and PO at pyrolysis temperatures of 350, 500 and 700°C are presented in Table (4) and Fig. (4). These parameters are critical indicators of the adsorptive and catalytic potential of biochars and closely reflect the feedstocks' physicochemical characteristics (Tables 1 and 2), thermal behavior (Fig. 2) and structural evolution (Fig. 3). Overall, increasing pyrolysis temperature enhanced both surface area and pore volume, primarily due to progressive volatile release and micro- and mesopore development (Zhao et al., 2013 and Ahmad et al., 2014). GSD-derived biochars showed the most pronounced increase, with BET surface area rising from 1.63 $m^2\ g^{-1}$ at 350°C to 47.59 $m^2\ g^{-1}$ at 700°C and pore volume from 0.008 $cm^3\ g^{-1}$ to 0.357 $cm^3\ g^{-1}$. This trend reflects GSD's moderate organic content and high ash levels, alongside increased aromaticity, as confirmed by FT-IR and TGA-DTA results. In contrast, PM-derived biochars exhibited a slower increase in BET surface area, reaching only 11.31 $m^2\ g^{-1}$ at 700°C, likely due to high ash and low FC content. However, pore volume rose significantly, from 0.055 to 0.606 $cm^3\ g^{-1}$, suggesting enhanced mesopore development. These findings are consistent with FT-IR results indicating partial degradation of aliphatic and polysaccharide structures and with literature noting limited porosity in PM biochars (Yin et al., 2017).

PO-derived biochars displayed a non-linear trend, with surface area increasing sharply from 1.92 $m^2\ g^{-1}$ at 350°C to 41.76 $m^2\ g^{-1}$ at 500°C, then declining to 21.20 $m^2\ g^{-1}$ at 700°C, despite continued growth in pore volume (from 0.287 to 1.002 $cm^3\ g^{-1}$). This suggests pore collapse or structural fusion at higher temperatures, as supported by SEM observations and similar findings by Downie et al. (2009) and Singh et al. (2022). The high carbon content and low nitrogen and sulfur levels in PO biochars (Table 2)

contributed to their favorable surface characteristics at 500 °C, reflecting efficient lignocellulosic conversion and aromatic structure development. Although the measured BET surface areas are lower than those of commercial activated carbons (500–1000 $m^2 g^{-1}$), they fall within the reported ranges for non-activated biochars (3–170 $m^2 g^{-1}$ for GSD, 1–20 $m^2 g^{-1}$ for PM, and 10–260 $m^2 g^{-1}$ for PO (Zhou et al., 2015 and Gupta et al., 2020). These properties make the biochars suitable for soil improvement, contaminant adsorption and water purification. For higher-performance applications, post-pyrolysis activation could be employed. Studies by Zaker et al. (2019) and Hossain et al. (2011) have shown that chemical or steam activation can significantly enhance surface area, with PO biochar reaching up to 899.33 $m^2 g^{-1}$ and GSD biochar up to 170 $m^2 g^{-1}$ under optimized conditions.

1.7. Scanning Electron Microscopy (SEM) analysis

The surface morphology of biochars derived from GSD, PM and PO was investigated using SEM, with representative micrographs at 700°C presented in Fig. (5). SEM analysis revealed significant morphological changes with increasing pyrolysis temperature, highlighting the progressive development of porosity and structural reorganization. At 700°C, all biochar samples exhibited distinct crack networks and fragmented surfaces-characteristic of extensive thermal degradation and volatile matter release. These surface features are consistent with the trends observed in TGA-DTA thermograms (Fig. 2), indicating significant devolatilization and with the reduction in functional groups shown in FT-IR spectra (Fig. 3). For GSD-derived biochar, SEM images displayed a highly porous and rough texture, marked by an intricate web of micro-cracks and channels. This morphological evolution corresponds to the sharp increase in BET surface area (from 1.63 $m^2 g^{-1}$ at 350°C to 47.59 $m^2 g^{-1}$ at 700°C) and pore volume (from 0.008 to 0.357 $cm^3 g^{-1}$), reflecting a well-developed porous network.

The moderate ash content and relatively high FC (Tables 1 and 2) contributed to matrix stability and pore preservation. PM-derived biochar also showed clear signs of fragmentation and pore formation at 700 °C, although the pore distribution appeared less uniform and more isolated compared to GSD. SEM images revealed scattered voids and surface ruptures, aligning with the moderate BET surface area increase (11.31 $m^2 g^{-1}$ at 700°C) and the significant rise in pore volume (0.606 $cm^3 g^{-1}$). This limited pore uniformity can be attributed to the low lignocellulosic content and high ash levels in PM (Table 1), which may restrict the development of an interconnected porous network (Yin et al., 2017).

Interestingly, PO-derived biochar demonstrated a contrasting behavior. At 500°C, SEM images revealed a well-developed porous structure with large, interconnected pores, corresponding with the sharp increase in BET surface area (41.76 $m^2 g^{-1}$) and moderate pore volume (0.024 $cm^3 g^{-1}$). However, at 700°C, the PO biochar surface became visibly denser and less

porous, with evidence of pore collapse or sintering. This morphological shift explains the observed reduction in BET surface area (to 21.20 m^2 g^{-1}) despite the continued increase in pore volume (1.002 cm^3 g^{-1}). Such behavior likely results from thermal fusion of mineral-rich components or partial graphitization, as suggested by Singh et al. (2022) and is further supported by FT-IR data indicating aromatic structure formation and the high carbon content of PO biochar (Table 2). The observed differences in SEM morphology across feedstocks also align with biochar yield trends (Table 3). PO biochar exhibited the highest initial yield but a sharper reduction at elevated temperatures, reflecting rapid devolatilization and structural transformation. In contrast, GSD and PM showed more gradual changes, maintaining more stable surface structures across the temperature range.

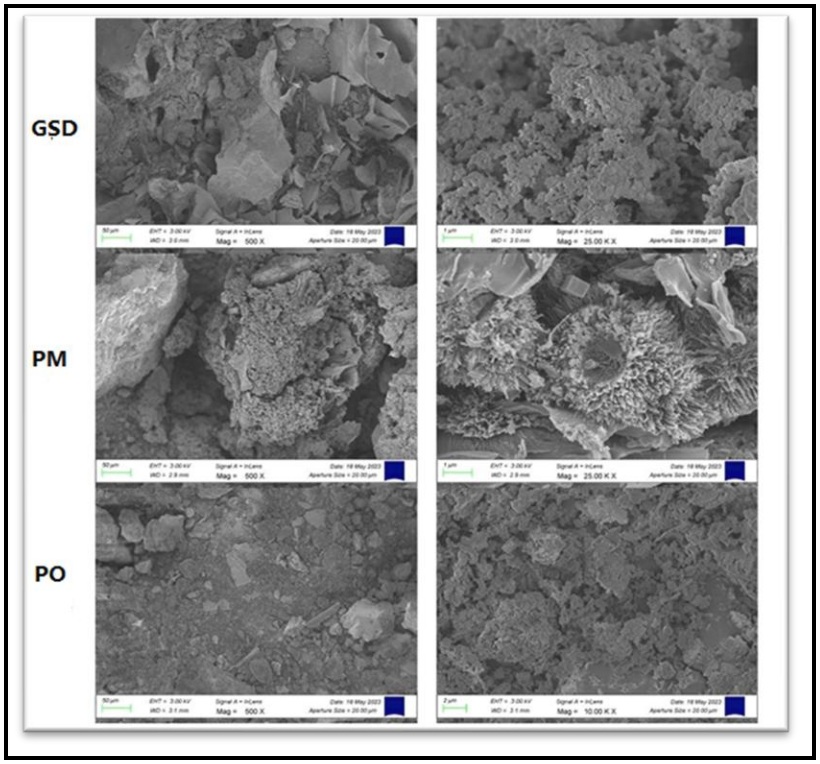

Fig. (5). SEM images of biochars derived from GSD, PM and PO at 700°C.

1.8. X-Ray Diffraction (XRD) analysis

The simulated XRD patterns of biochars produced from GSD, PM, and PO at 350, 500 and 700°C (Fig. 6) provide insights into the crystalline and amorphous transformations that occur during pyrolysis. These structural changes are closely linked to thermal degradation behavior (Fig. 2), mineral content (Tables 1 and 2), surface characteristics (Table 4 and Fig. 4) and

morphological features (Fig. 5). At 350°C, GSD biochar exhibited a broad amorphous hump centered around ≈22° 2θ in the XRD pattern, characteristic of disordered carbonaceous structures and indicating a low degree of crystallinity. Additionally, weak diffraction peaks corresponding to quartz (SiO_2) and calcite ($CaCO_3$) were observed, reflecting the inherent mineral composition of the feedstock (Zhao et al., 2013 and Shaaban et al., 2014). These findings are typical for low-temperature biochars derived from manure-based materials, where incomplete carbonization and residual mineral phases coexist within the biochar matrix. As temperature increases to 500 and 700°C, these peaks become sharper and more intense. Notably, calcium oxide (CaO) appears at 700°C due to the thermal decomposition of calcite, as also reported by Cantrelle al. (2012) and Suliman et al. (2016), who found that high-temperature pyrolysis promotes crystallization of mineral constituents in animal manure biochars.

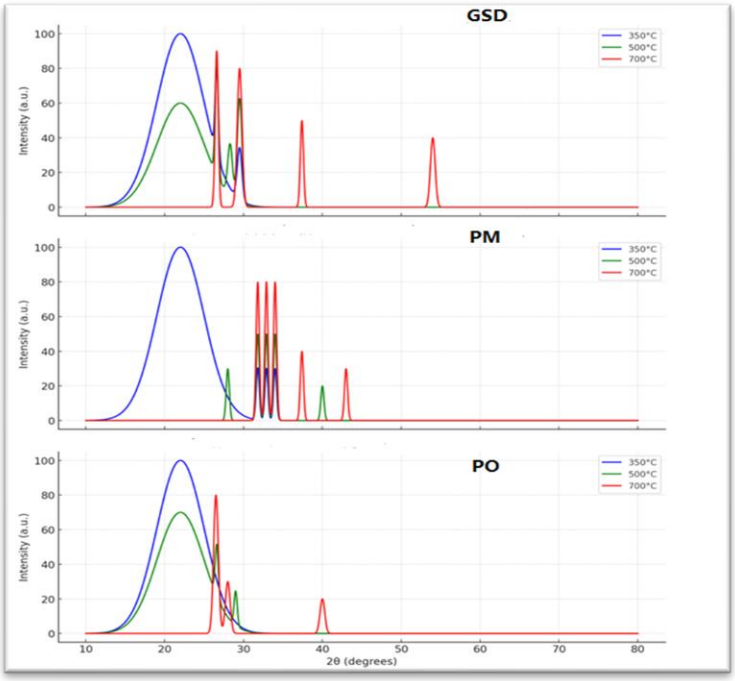

Fig. (6). XRD patterns of GSD, PM and PO biochars at 350 °C, 500 °C, and 700 °C.

PM biochar XRD patterns show increasing crystallinity with temperature. Peaks near 31.8°, 32.9° and 34.0° indicate the formation of hydroxyapatite [$Ca_5(PO_4)_3OH$], which intensifies at higher temperatures. These results match the findings of Yuan et al. (2011) and Fang et al. (2014), which reported dominant hydroxyapatite phases in poultry manure biochars and emphasized their thermal stability above 500°C. Additional reflections

from alkali salts such as KCl or K_2SO_4 are common in poultry-derived biochars due to high potassium content. PO-derived biochar shows mostly amorphous features at 350°C, with increasing ordering as pyrolysis temperature rises. At 500°C, weak peaks from quartz and potassium carbonate (K_2CO_3) appear, while at 700°C, a distinct peak around 26.5° 2θ emerges, indicating the formation of graphitic carbon planes, a sign of partial graphitization. These changes are supported by the study of Keiluweit et al. (2010) and Singh et al. (2022), who observed structural ordering and increased aromaticity in lignocellulosic biochars at high temperatures.

1.9. X-Ray Fluorescence (XRF) analysis of feedstocks and derived biochars

XRF analysis revealed significant compositional differences between the raw feedstocks (GSD, PM and PO) and their respective biochars, highlighting the impact of both feedstock origin and pyrolysis temperature on elemental concentration patterns (Fig. 7 and 8). PM displayed the highest levels of calcium (Ca), phosphorus (P) and potassium (K) in its raw state, primarily due to poultry dietary supplements, as supported by Yuan et al. (2011).

Following pyrolysis, PM biochars showed marked increases in Ca and P concentrations, with XRF spectra indicating the formation of thermally stable minerals like hydroxyapatite (Fang et al., 2014). The retention of K, even after high-temperature treatment, aligns with its known low volatility below 700°C (Cantrell et al., 2012), enhancing the fertilizer value of PM biochar. PO, in contrast, was characterized by elevated silicon (Si) levels, likely resulting from its lignocellulosic composition and possible soil contamination during collection, a trend consistent with Domingues et al. (2017), who observed similar Si enrichment in olive-based biochar. After pyrolysis, Si content remained relatively stable, with slight peak intensification, suggesting the thermal stability of silica-related compounds. Additionally, the concentration of K increased, enhancing its potential as a soil amendment. GSD showed intermediate elemental profiles with higher magnesium (Mg) and iron (Fe) compared to PO and PM. Pyrolysis caused noticeable Fe enrichment in GSD biochar, which is beneficial for environmental applications such as heavy metal sorption (Inyang et al., 2016).

Additionally, the Si content in PO remained stable post-pyrolysis, with only slight intensification in peak height. For all feedstocks, XRF results confirmed a concentration effect post-pyrolysis due to mass loss from organic matter volatilization. This is reflected by the higher intensity of elemental peaks in biochars compared to raw materials (Fig. 8), especially at elevated temperatures like 700°C. Micronutrients such as manganese (Mn), zinc (Zn) and copper (Cu) were notably more concentrated in PM feedstocks, a trend that was further accentuated in the biochar form. The presence of Zn and Cu in PM is typically linked to dietary additives in poultry production (Chanaka et al., 2022) and these elements are known to be retained in char structures

during pyrolysis due to their low vapor pressures at moderate temperatures. However, trace heavy metals such as lead (Pb), though present at low levels, were also enriched post-pyrolysis, underscoring the need for caution regarding long-term soil application (Lu et al., 2015). Overall, the XRF elemental enrichment patterns directly reflect both the initial feedstock composition and the thermal stability of each element at increasing pyrolysis temperatures. PM biochars demonstrated the highest nutrient density, GSD biochars showed balanced mineral enrichment with high Fe content and PO biochars retained key macronutrients like K and Si while offering high carbon content and structural stability (Hossain et al., 2011; Novak et al., 2013 and Domingues et al., 2017). These results align with the broader literature (Ronsse et al., 2013) and confirm the critical role of feedstock selection and pyrolysis conditions in tailoring biochar properties for specific soil or environmental applications.

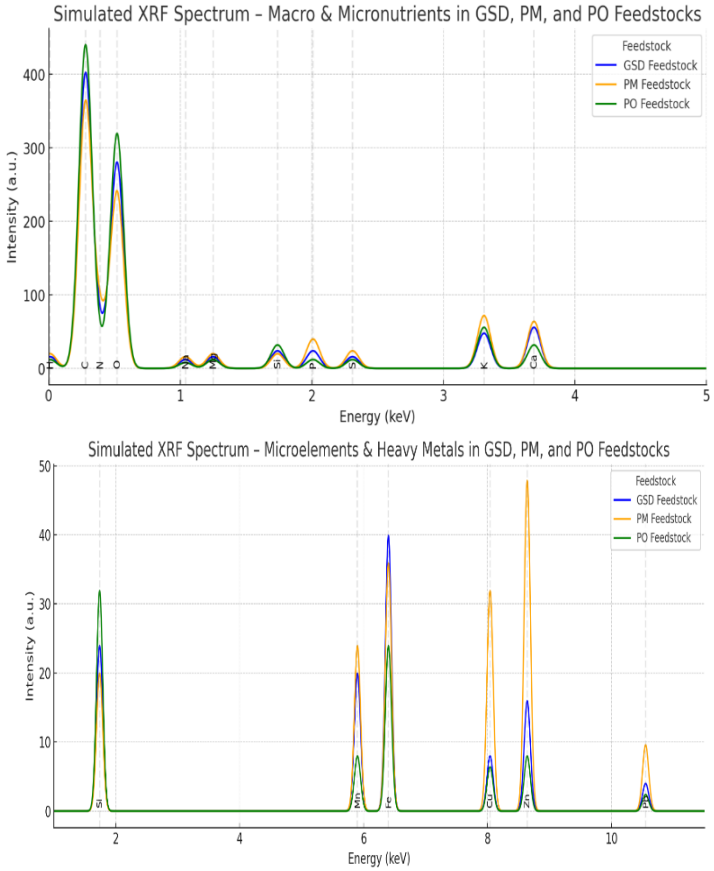

Fig. (7). Simulated XRF Spectra of macro, micronutrients and heavy metals in GSD, PM and PO feedstock**.**

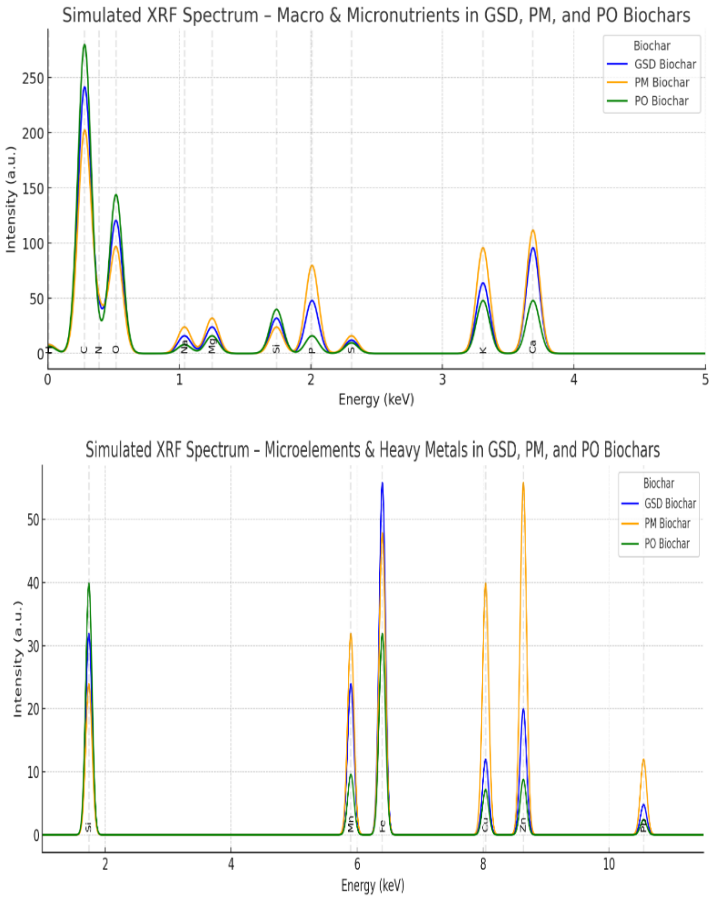

Fig. (8). Simulated XRF Spectra of macro, micronutrients and heavy metals in GSD, PM and PO bichars pyrolyzed at 700°C.

1.10. Physiochemical properties of feedstocks and derived biochars

Table (5) provides the changes in physicochemical properties of GSD, PM and PO during pyrolysis at 350, 500 and 700°C. The results illustrate a progressive trend of chemical stabilization, mineral concentration and structural transformation as pyrolysis temperature increases, all of which significantly affect biochar functionality. CEC increased notably with pyrolysis temperature across all feedstocks. GSD increased from 35 cmol kg^{-1} in the raw material to 85 cmol kg^{-1} at 700°C, PM increased from 45 to 100 cmol kg^{-1} and PO from 30 to 70 cmol kg^{-1}. This trend reflects the gradual development of oxygen-containing surface functional groups and enhanced porosity, which improve cation adsorption capacity (Liang et al., 2006 and Lehmann et al., 2011). The higher final CEC observed in PM biochar is further attributed to its elevated ash content (Table 1), which contributes basic oxides

and reactive mineral phases such as hydroxyapatite, as corroborated by XRD analysis and the findings of Fang et al. (2014).

Table (5). Estimated physiochemical properties of feedstocks and derived biochars at different pyrolysis temperatures.

Sample	Temp. (°C)	CEC (cmol kg^{-1})	EC (1:10) (dS m^{-1})	pH 1:10	TOC (% w w^{-1})	TON (% w w^{-1})	C/N Ratio	Density (g cm^{-3})
GSD (Feedstock)	–	35	1.80	7.8	38.5	3.8	10.1	0.82
GSD (Biochar)	350	55	1.20	8.0	44.5	2.5	17.8	0.65
	500	70	0.85	8.2	48.0	1.8	26.7	0.52
	700	85	0.60	8.4	52.0	1.2	43.3	0.42
PM (Feedstock)	–	45	2.50	7.6	32.7	4.7	7.0	0.89
PM (Biochar)	350	70	1.60	8.0	38.0	2.9	13.1	0.67
	500	85	1.00	8.2	40.0	1.9	21.1	0.58
	700	100	0.90	8.3	41.5	1.4	29.6	0.51
PO (Feedstock)	–	30	1.10	6.9	40.6	2.0	20.3	0.71
PO (Biochar)	350	50	0.80	7.6	46.0	1.4	32.9	0.52
	500	60	0.60	8.0	50.0	0.9	55.6	0.42
	700	70	0.50	8.2	53.0	0.6	88.3	0.36

Note: GSD = Goat-Sheep Dung, PM = Poultry Manure, PO = Olive Pomace

In contrast, EC declined progressively with increasing pyrolysis temperature. PM, which exhibited the highest initial EC (2.50 dS m^{-1}), dropped to 0.90 dS m^{-1} at 700°C. Similarly, GSD and PO decreased from 1.80 and 1.10 to 0.60 and 0.50 dS m^{-1}, respectively. This decline is primarily attributed to the volatilization of low-molecular-weight soluble salts during pyrolysis, especially at temperatures exceeding 500°C (Ronsse et al., 2013). Lower EC values are beneficial when applying biochar to soils, as they reduce the risk of salt-induced stress in plants, as noted by Novak et al. (2009). pH values followed an increasing trend with pyrolysis temperature, transitioning from near-neutral or slightly acidic values in raw feedstocks to alkaline levels at higher temperatures. PO shifted from pH 6.9 to 8.2 at 700°C. This alkalinization results from the accumulation of alkaline ash constituents (Ca, Mg and K) and the thermal loss of acidic functional groups such as carboxyl and phenolic groups (Yuan et al., 2011). The most significant pH increases were observed between 350 and 500°C, aligning with trends reported for similar biomass types (Cantrell et al., 2012).

TOC content also increased with pyrolysis temperature, reflecting enhanced carbonization and aromatic condensation. GSD TOC rose from 38.5 to 52.0%, PM from 32.7 to 41.5% and PO from 40.6 to 53.0%. These increases correspond to the progressive degradation of labile organic matter and the formation of stable carbonaceous structures (Domingues et al., 2017), as

confirmed by FT-IR and TGA analyses. Notably, PO maintained the highest TOC across all temperatures, confirming its lignocellulosic nature and superior carbon retention (Zhao et al., 2013).

Conversely, TON declined sharply with rising temperature, particularly between 350 and 700°C, due to the volatilization of nitrogen-containing compounds (e.g., NH_3, NO_2 and HCN), a widely documented phenomenon in pyrolysis processes (Steiner et al., 2007). PM's TON dropped from 4.7 to 1.4%, GSD from 3.8 to 1.2%, and PO from 2.0 to 0.6%. Consequently, biochars become poor sources of plant-available nitrogen and should be supplemented with nitrogen fertilizers when used for soil fertility enhancement. As a direct result of TOC enrichment and TON loss, the C/N ratio increased dramatically with temperature. PO exhibited the highest final C/N ratio, rising from 20.3 in the raw state to 88.3 at 700°C, followed by GSD (43.3) and PM (29.6). These elevated C/N ratios signify high carbon stability but may also slow microbial decomposition and nitrogen be cycling in soils (Bruun et al., 2012). Finally, density consistently decreased with increasing pyrolysis temperature due to the development of internal pores, formation of cracks and overall mass loss from volatile component release. GSD's density declined from 0.82 to 0.42 g cm^{-3}, PM from 0.89 to 0.51 g cm^{-3} and PO from 0.71 to 0.36 g cm^{-3}. This reduction in density is well-supported by SEM and BET results, which show corresponding increases in pore volume and surface area, particularly at 700°C (Downie et al., 2009). While lower-density biochars are advantageous for improving soil aeration and structure, they may require higher application rates to achieve uniform field distribution.

2. Effects of Biochar on Soil Chemical and Physical Properties at pyrolysis 500°C Temperature

The 60-day greenhouse incubation study investigating the effects of biochars produced at 500 °C from GSD, PM and PO, applied at 2 and 5% (w w^{-1}) rates, revealed significant improvements in multiple soil physicochemical properties (Table 6). Soil pH increased significantly in all biochar-amended treatments compared to the control (pH 7.6), with the highest values recorded for GSD-5% and PM-5% treatments (pH 8.2).

This alkalization can be attributed to the inherently alkaline nature of the biochars, resulting from the accumulation of basic cations (Ca^{2+}, Mg^{2+} and K^{+}) in the ash fraction. As shown in Table (5), biochars pyrolyzed at 500°C displayed elevated pH values (8.0-8.4), reflecting the presence of carbonates and mineral oxides formed during thermal decomposition. These findings align with the reports of Yuan et al. (2011) and Novak et al. (2009), who observed that pyrolysis temperatures above 400°C promote the formation of mineral carbonates and oxides phases that increase soil pH. Regarding EC, PM-derived biochars exhibited the highest EC values (1.10 dS m^{-1} at 2% application rate), reflecting their elevated ash content (28.60%) as mentioned in Table (1) and high levels of nitrogen and soluble ions (Table 2).

Table (6). Soil physicochemical properties after 60-day incubation with biochars pyrolyzed at 500°C and applied at 2 and 5% (w w^{-1}).

Treatment	pH (1:2.5)	EC (1:2.5) (dS/m)	TOC (%)	TON (%)	C/N ratio	CEC (cmol kg^{-1})	Bulk Density (g cm^{-3})	Porosity (%)	AWC (%)
Control	7.6 ± 0.05**c**	0.85 ± 0.01**b**	38.5 ± 0.8**d**	3.8 ± 0.2**a**	10.13 ± 0.3**d**	35 ± 1.2**d**	1.52 ± 0.02**a**	42.64 ± 1.1**c**	7.8 ± 0.3**c**
GSD-2%	8.1 ± 0.04**ab**	0.88 ± 0.02**b**	45.5 ± 1.1**bc**	2.1 ± 0.1**b**	21.70 ± 0.7**c**	62 ± 1.9**c**	1.48 ± 0.01**ab**	43.99 ± 1.4**bc**	11.0 ± 0.4**b**
GSD-5%	8.2 ± 0.03**a**	0.85 ± 0.02**b**	48.0 ± 1.2**b**	1.8 ± 0.1**b**	26.70 ± 0.8**b**	70 ± 2.1**b**	1.44 ± 0.01**b**	45.66 ± 1.5**b**	12.5 ± 0.5**b**
PM-2%	8.1 ± 0.05**ab**	1.10 ± 0.03**a**	38.5 ± 1.0**d**	2.2 ± 0.1**b**	17.50 ± 0.6**c**	75 ± 2.2**b**	1.45 ± 0.01**b**	45.28 ± 1.3**b**	10.0 ± 0.4**bc**
PM-5%	8.2 ± 0.04 **a**	1.00 ± 0.03**a**	40.0 ± 0.9**c**	1.9 ± 0.1**b**	21.10 ± 0.6**c**	85 ± 2.5**a**	1.40 ± 0.01**b**	47.17 ± 1.4**b**	11.3 ± 0.4**b**
PO-2%	7.9 ± 0.03**b**	0.65 ± 0.01**c**	48.0 ± 1.3**ab**	1.1 ± 0.05**c**	43.60 ± 1.4**b**	55 ± 1.6**d**	1.42 ± 0.01b	46.43 ± 1.3**ab**	12.8 ± 0.5**ab**
PO-5%	8.0 ± 0.02**ab**	0.60 ± 0.01**c**	50.0 ± 1.1**a**	0.9 ± 0.05**c**	55.60 ± 1.5**a**	60 ± 1.8**c**	1.38 ± 0.01**c**	47.92 ± 1.7**a**	14.2 ± 0.6**a**

Note: Values are presented as mean ± standard deviation. Different letters within columns indicate significant differences ($p < 0.05$) based on Tukey's HSD test.

In contrast, PO-derived biochars resulted in significantly lower EC values (0.60–0.65 dS m^{-1}), which is beneficial for soils vulnerable to salinity stress. These observations highlight the importance of feedstock selection when tailoring biochar amendments for site-specific soil management goals.

Biochar application also resulted in substantial increases in TOC, especially in the PO-5% treatment, which reached 50.0%; the highest among all treatments. This enhancement reflects PO's high FC content (Table 1), superior thermal stability (Table 2) and its favorable textural properties; most notably, the highest BET surface area at 500 °C (41.76 m^2 g^{-1}) as shown in Table (4).

The increased surface area may promote the physical protection of soil organic matter through micropore entrapment and reduced microbial decomposition, thereby enhancing TOC retention (Lehmann et al., 2006 and Mukherjee et al., 2011). While GSD and PM biochars also improved TOC compared to the control, their effects were less pronounced due to their comparatively lower carbon content and smaller surface areas. In contrast, TON decreased across all biochar treatments compared to the control (3.8%), with the most substantial reduction observed in the PO-5% treatment (0.9%). This decrease is attributed to the inherently low nitrogen content in PO (1.90%) as in Table (2) and its high carbon content, resulting in elevated C/N ratios (up to 55.6). Such high ratios suggest limited nitrogen mineralization and potential short-term nitrogen immobilization, especially under microbial demand. These findings are consistent with Glaser et al. (2002), who reported that biochars rich in carbon but low in nitrogen can temporarily reduce soil nitrogen availability, emphasizing the need for nitrogen supplementation during the early stages of biochar application.

CEC improved markedly in all biochar-amended soils. The highest CEC was recorded in PM-5% (85 cmol kg^{-1}), followed by GSD-5% (70 cmol kg^{-1}) and PO-5% (60 cmol kg^{-1}), all significantly higher than the control (35 cmol kg^{-1}). This enhancement is attributed to the presence of oxygen-containing surface functional groups (–COOH, –OH) and increased porosity from thermal decomposition. As shown in Table (5), biochars exhibited higher CEC than their respective raw feedstocks. Additionally, BET and pore volume data (Table 4) confirm that biochars, particularly those from PO and GSD, developed significant porosity that facilitates nutrient adsorption. These results are in line with Liang et al. (2006) and Keiluweit et al. (2010), who noted that biochars with higher aromaticity and oxidized functional groups provide more reactive sites for nutrient retention and cation exchange. Biochar treatments also significantly reduced soil bulk density while increasing soil porosity. The PO-5% treatment resulted in the lowest soil bulk density (1.38 g cm^{-3}) and the highest porosity (47.92%), reflecting PO's low inherent biochar density (0.42 g cm^{-3}) as mentioned in Table (5) and its moderate pore volume (0.024 cm^3 g^{-1}) as shown in Table (4). These structural changes are beneficial for improving soil aeration, water infiltration and root penetration, especially

in compacted or degraded soils (Downie et al., 2009 and Abel et al., 2013). GSD and PM biochars also reduced bulk density and increased porosity, with stronger effects at the 5% application rate, further supporting biochar's role as a structural soil amendment. Available water content (AWC) followed a similar trend. The PO-5% treatment exhibited the highest AWC (14.2%), compared to 7.8% in the control. This improvement is linked to PO biochar's mesoporous structure and enhanced surface functionality, both of which increase soil water-holding capacity. The higher AWC observed in PO-amended soils is supported by BET surface area data and consistent with findings from Abel et al. (2013), who reported that biochars with well-developed pore networks improve soil water retention. GSD and PM biochars also enhanced AWC, although to a lesser extent, reflecting differences in feedstock properties and pyrolysis behavior.

CONCLUSION

This comprehensive study evaluated the impact of feedstock type and pyrolysis temperature on biochar properties and their subsequent effects on the physicochemical characteristics of sandy soils in the El-Hammam region, Egypt. Three locally available agricultural residues: PO, GSD and PM; ere pyrolyzed at 350°C, 500°C and 700°C to produce biochars with distinct physicochemical profiles. Thermal analyses (TGA-DTA), proximate and ultimate compositions, FT-IR spectroscopy, BET surface area, SEM, XRD and XRF collectively demonstrated that both feedstock composition and pyrolysis temperature significantly influenced biochar quality in terms of carbon stability, surface area, porosity, nutrient content and mineral composition. Biochars produced at 500°C were selected as the optimal treatment temperature due to their balanced structural stability, nutrient retention, surface functionality and moderate yield. These biochars were applied to El-Hammam sandy soil at two amendment rates (2% and 5% w w^{-1}). Among the feedstocks, PO biochar at a 5% application rate showed the most pronounced improvements in soil quality by enhancing TOC, soil porosity and available water content (AWC), thus contributing to better soil structure, moisture retention and carbon sequestration potential. PM biochar exhibited the highest enhancement in CEC and nutrient availability, primarily due to its high ash content and elevated macronutrient concentrations (N, P and K), making it highly suitable for nutrient-deficient soils. GSD biochar provided balanced, moderate improvements in multiple soil parameters, making it a multifunctional amendment option. Overall, this research confirms that the performance of biochar as a soil amendment is highly dependent on both the choice of feedstock and the pyrolysis conditions. The study highlights that olive pomace biochar at 500°C and 5% application rate represents the most effective strategy for improving the fertility and physical quality of degraded sandy soils under arid and semi-arid climatic conditions such as those found

in El-Hammam. The findings also emphasize the broader environmental and agricultural benefits of biochar production from local agricultural waste; offering a sustainable solution for organic waste management, soil rehabilitation, and climate change mitigation through carbon sequestration. Further long-term field trials, economic feasibility studies and crop productivity assessments are recommended to validate these findings at larger scales and across varying environmental conditions.

REFERENCES

Abdel-Rahman, M., M.A. Abu-Elgheit and R. Zewail (2022). Improving soil water retention and fertility in arid regions using biochar. Arid Land Research and Management, 36 (4): 415-433.

Abel, S., A. Peters, S. Trinks, H. Schonsky, M. Facklam and G. Wessolek (2013). Impact of biochar and hydrochar on physical properties of loamy soil. Geoderma, 199: 183-190.

Ahmad, M., S.S. Lee, X. Dou, D. Mohan, J.K. Sung, J.E. Yang and Y.S. Ok, (2014). Effects of pyrolysis temperature on soybean stover-and peanut shell-derived biochar properties and sorption of copper and lead in aqueous solutions. Bioresource Technology, 118: 536-544.

Ahmed, B., K.A. Alaboudi and G. Brodie (2019). Effect of biochar on Pb, Cd, and Cr availability and maize growth in artificial contaminated soil. Annals of Agricultural Sciences, 64 (1): 95–102. https://doi.org/10.1016/j.aoas.2019.04.002

Al-Wabel, M.I., Q. Hussain, A.R.A. Usman, M. Ahmad, A.S. Al-Farraj and Y.S. Ok (2019). Impact of biochar properties on soil conditions and agricultural sustainability: A review. Land Degradation & Development, 30 (7): 1721-1740.

Antal, M.J. and M. Grønli (2003). The Art, Science, and Technology of Charcoal Production. Industrial & Engineering Chemistry Research, 42 (8): 1619-1640.

AOAC (2000). Official Methods of Analysis of AOAC International (17th. ed., Vols. 1 & 2). Gaithersburg, MD, USA: Association of Official Analytical Chemists. Washington, DC.

ASTM (2018). ASTM D4239-18e1: Standard Test Method for Sulfur in the Analysis Sample of Coal and Coke Using High-Temperature Tube Furnace Combustion. West Conshohocken, PA: ASTM International. Available online at: https://doi.org/10.1520/D4239-18E01

ASTM (2019). ASTM E872-82(2019): Standard Test Method for Volatile Matter in the Analysis of Particulate Wood Fuels. West Conshohocken, PA: ASTM International. Available online at: https://doi.org/10.1520/E0872- 82R19.2

ASTM (2020). ASTM E1755-01(2020): Standard Test Method for Ash in Biomass. West Conshohocken, PA: ASTM International. Available online at: https://doi.org/10.1520/E1755-01R20.2

ASTM (2021). ASTM D5373-21: Standard Test Methods for Determination of Carbon, Hydrogen, and Nitrogen in Analysis Samples of Coal and Carbon. West Conshohocken, PA: ASTM International. Available online at: https://doi.org/10.1520/D5373-21

Awasthi, M.K. (2020). Effect of feedstock characteristics on biochar properties and its application in remediation. Bioresource Technology, 297: 122396.

Basu, P. (2013). Biomass Gasification, Pyrolysis and Torrefaction. In 'Practical Design and Theory (2nd ed.)'. London, UK, Academic Press.

Blake, G.R., and K.H. Hartge (1986). Bulk density. In 'A. Klute (Ed.), Methods of Soil Analysis: Part 1-Physical and Mineralogical Methods (2nd ed.)'. Madison, WI: Soil Science Society of America., pp. 363–375.

Bremner, J.M. and C.S. Mulvaney (1982). Nitrogen—Total. In 'A.L. Page (Ed.), Methods of Soil Analysis: Part 2-Chemical and Microbiological Properties (2nd. ed.)'. Madison, WI: ASA and SSSA, pp. 595-624.

Bruun, E.W., H. Hauggaard-Nielsen, N. Ibrahim, H. Egsgaard, P. Ambus, P.A. Jensen and K. Dam-Johansen (2012). Influence of fast pyrolysis temperature on biochar labile fraction and short-term carbon loss in a loamy soil. Biomass and Bioenergy, 35 (3): 1182-1189.

Cantrell, K.B., P.G. Hunt, M. Uchimiya, J.M. Novak, K.S. Ro and M. Ahmedna, (2012). Impact of pyrolysis temperature and manure source on physicochemical characteristics of biochar. Bioresource Technology, 107: 419-428.

Carrier, M., A. Loppinet-Serani, D. Denux, J.M. Lasnier, F. Ham-Pichavant, F. Cansell and C. Aymonier (2011). Thermogravimetric analysis as a new method to determine the lignocellulosic composition of biomass. Biomass and Bioenergy, 35 (1): 298-307.

Cely, P., K.B. Cantrell, J.M. Novak, K.S. Ro amd D.A. Laird (2015). Characterization of biochar from poultry manure and its potential as a soil amendment. Journal of Analytical and Applied Pyrolysis, 111: 193-204.

Chanaka, U.N.W.B., S.B. Navaratne and W.T.S.P. Premachandra (2022). Heavy-metal accumulation in poultry manure and potential health implications: A review. Environmental Science and Pollution Research, 29 (17): 25616-25634.

Chen, Y., X. Xiao and B. Chen (2017). Structural evolution of biochar from biomass pyrolysis and its correlation with pyrolysis temperature: A review. Bioresource Technology, 223: 139-147.

Chen, H., X. Yuan, S. Zhou, X. Chen and Y. Wu (2021). Impacts of poultry manure-derived biochars on soil characteristics and plant growth: A review. Chemosphere, 263: 128190.

Chen, W.H., P.C. Kuo and S.H. Liu (2016). Thermal behavior and decomposition kinetics of woody biomass torrefaction. Energy, 113: 1075-1084.

Chen, W.H., S.C. Ye and H.K. Sheen (2012). Hydrothermal carbonization of sugarcane bagasse via wet torrefaction in association with microwave heating. Bioresource Technology, 118: 195.

Domingues, R.R., P.F. Trugilho, C.A. Silva, J. de Oliveira Júnior, R.C., Patrocínio and M.G.A. Korn (2017). Characterization of bio-oil and biochar from slow pyrolysis of lignocellulosic residues. Renewable Energy, 112: 247-257.

Downie, A., A. Crosky and P. Munroe (2009). Physical Properties of Biochar. In 'Lehmann, J. and S. Joseph (Eds.), Biochar for Environmental Management: Science and Technology'. London, UK: Earthscan, Taylor and Francis, pp. 13-32.

El-Beltagy, A.E., F.H. Abdel-Rahman and S.R. Mahrous (2023). Effectiveness of different biochars on water retention and nutrient availability in sandy soils of arid regions. Journal of Arid Environments, 205: 104808.

El-Gohary, H.M., A.H. Said and S. Ibrahim (2023). Context-specific evaluation of biochar benefits in Egyptian soils. Journal of Soil and Water Conservation, 78 (3): 150-161.

El-Shafie, A.I., F. Khalil and M.A. Youssef (2022). Organic waste accumulation in El-Hammam region: sources, management and conversion possibilities. Egyptian Journal of Agricultural Research, 100 (2): 567-582.

Fang, Y., B.P. Singh, B. Singh, E. Krull and C. Chen (2014). Biochar carbon stability in four contrasting soils. European Journal of Soil Science, 65 (1): 60-71.

FAO (2021). Food and Agriculture Organization of the United Nations Biochar fertilizer. FAO TECA, Rome. Available online at: https://doi.org/10.4060/cb7085en

Gao, S., M., Wang and Y. Zhang (2020). Insights into the properties and potential applications of poultry manure biochar. Waste Management, 110: 163-172.

García-Maraver, A., M. Zamorano, H. Pérez, R. Padilla and J.L. Valverde (2010). Combustion and thermogravimetric analysis of olive pomace in a conventional combustor. Fuel, 89 (10): 2841-2849.

Glaser, B., J. Lehmann, J. W. Zech (2002). Ameliorating physical and chemical properties of highly weathered soils in the tropics with charcoal: A review. Biology and Fertility of Soils, 35 (4): 219-230.

Gupta, N., H.W. Kua and D.H.L. Ng (2019). Biochar production and characterization from the pyrolysis of horticultural waste biomass in Singapore. Environmental Science and Pollution Research, 26: 7926-7938.

Gupta, A., R.J. Jadhav and J. Bhattacharya (2020). Activated carbon from biomass for water treatment: A review. Journal of Environmental Chemical Engineering, 8 (5): 103607.

Hassan, M.K., Y.J. Liu, R. Naidu, S.J. Parikh, J.H. Du and F.J. Qi (2020). Influences of feedstock sources and pyrolysis temperature on the properties of biochar and functionality as adsorbents: A meta-analysis. Science of the Total Environment, 744*:* 140714.

Hassan, O.M., A.E. Ahmed and S.A. Hassan (2021). Physical and chemical characterization of olive-pomace biochar and its soil effectiveness. Waste and Biomass Valorization, 12 (5): 2375-2387.

Hossain, M.K., V. Strezov, K.Y. Chan, A. Ziolkowski and P.F. Nelson (2011). Influence of pyrolysis temperature on production and nutrient properties of wastewater sludge biochar. Journal of Environmental Management, 92 (1): 223-228.

Hu, Y., P.Y. Li, Y.P. Yang, M. Ling and X.F. Li (2022). Preparation and characterization of biochar from four types of waste biomass under matched conditions. BioResources, 17 (4): 6464-6475.

IBM Corp. (2017). IBM SPSS Statistics for Windows, Version 25.0. Armonk, NY: IBM Corp.

Inyang, M., B. Gao, P. Pullammanappallil, W. Ding and A.R. Zimmerman (2016). Biochar from anaerobically digested sugarcane bagasse. Bioresource Technology, 101 (22): 8868-8872.

Jeffery, S., D. Abalos, K.A. Spokas and F.G.A. Verheijen (2017). Biochar effects on crop yield. In 'J. Lehmann & S. Joseph (Eds.), Biochar for environmental management: Science, technology and implementation', Routledge (2nded.), pp. 301-325.

Keiluweit, M., P,S. Nico, M.G. Johnson and M. Kleber (2010). Dynamic molecular structure of plant biomass-derived black carbon (biochar). Environmental Science & Technology*,* 44 (4): 1247-1253.

Klute, A. (1986). Water Retention: Laboratory Methods. In 'A. Klute (Ed.), Methods of Soil Analysis: Part 1—Physical and Mineralogical Methods (2nd. ed.)'. Soil Science Society of America, pp. 635-662.

Kumar, S., et al. (2020). Environmental impact of uncontrolled open burning of agricultural residues. Science of the Total Environment, 704, 135310. https://doi.org/10.1016/j.scitotenv.2019.135310

Lehmann, J. and S. Joseph (Eds.). (2015). Biochar for environmental management In 'Science, technology and implementation' (2nd. ed.). Routledge. DOI: 10.4324/9780203762264

Lehmann, J., J. Gaunt and M. Rondon (2006). Bio-char sequestration in terrestrial ecosystems: A review. Mitigation and Adaptation Strategies for Global Change, 11 (2): 403-427.

Lehmann, J., M.C. Rillig, J. Thies, C.A. Masiello, W.C. Hockaday and D. Crowley (2011). Biochar effects on soil biota - A review. *Soil Biology and* Biochemistry, 43 (9): 1812-1836.

Liang, B., J. Lehmann, D. Solomon, J. Kinyangi, J. Grossman et al. (2006). Black carbon increases cation exchange capacity in soils. Soil Science Society of America Journal, 70 (5): 1719-1730.

Lowell, S., J.E, Shields, M.A. Thomas and M. Thommes (2014). Characterization of Porous Solids and Powders. In 'Surface Area, Pore Size and Density (2nd. Ed.)'. Springer. Available online at: https://doi.org/10.1007/978-94-017-8663-9

Lu, K., X. Yang, J. Shen, B. Robinson, H. Huang et al. (2015). Effect of bamboo and rice straw biochars on the mobility and bioavailability of heavy metals in a multi-metal contaminated soil. Science of the Total Environment, 521-522: 28-35.

Mahmoud, S.H. and A.H. Abd-Elrahman (2025). Salinity impacts on soil and agricultural productivity in the Northwestern Coastal Zone of Egypt. Land Degradation and Development, 36 (3): 219-230.

Mahmoud, A., M.M. Shendi, B. Pradhan and F. Attia (2009). Utilization of remote sensing data and GIS tools for land use sustainability analysis: Case study in El Hammam area, Egypt. Open Geosciences, 1 (3): 347-367.

Méndez, A., A. Gómez, J. Paz-Ferreiro and G. Gascó (2013). Effects of sewage sludge biochar on plant metal availability after application to a Mediterranean soil. Chemosphere, 89 (11): 1354-1359.

Mukherjee, A., A.R. Zimmerman and W. Harris (2011). Surface chemistry variations among a series of laboratory-produced biochars. *Geoderma*, 163 (3-4), 247-255.

Munawar, M.A., A.H. Khoja, S.R. Naqvi, M.T. Mehran, M. Hassan, R. Liaquat and U.F. Dawood (2021). Challenges and opportunities in biomass ash management and its utilization in novel applications. Renewable and Sustainable Energy Reviews, 150: 111451.

Nelson, D.W. and L.E. Sommers (1996). Total Carbon, Organic Carbon, and Organic Matter. In 'D.L. Sparks (Ed.), Methods of Soil Analysis: Part 3: Chemical Methods Soil Science Society of America', American Society of Agronomy, pp. 961-1010. Available online: https://doi.org/10.2136/sssabookser5.3.c34

Novak, J.M., W.J. Busscher, D.L. Laird, M. Ahmedna, D.W. Watts and M. Niandou (2009). Impact of biochar amendment on fertility of a southeastern Coastal Plain soil. Soil Science, 174 (2): 105-112.

Novak, J.M., I.M. Lima, B. Xing, J.W. Gaskin, C. Steiner et al. (2013). Characterization of designer biochar produced at different

temperatures and their effects on a loamy sand. Annals of Environmental Science, 7 (1): 295-302.

Otero, M., M.J. Díaz, A. Morán and C. García (2002). Composting of cattle manure unsolid fraction: Chemical evolution and agronomic value of the compost. Bioresource Technology, 85 (2): 127-133.

Quiroga, G., L. Castrillón, Y. Fernández-Nava and E. Marañón (2010). Physico-chemical analysis and calorific values of poultry manure. Waste Management, 30 (5): 880-884.

Rajkovich, S., A. Enders, K. Hanley, C. Hyland, A.R. Zimmerman and J. Lehmann (2012). Corn growth and nitrogen nutrition after additions of biochars with varying properties to a temperate soil. Biology and Fertility of Soils, 48 (3): 271-284.

Reynolds, W.D., D.E. Elrick, E.G. Youngs, A. Amoozegar, H.W.G. Booltink and J. Bouma (2002). Saturated and Field-Saturated Water Flow Parameters. In 'Dane. J.H. and G.C. Topp (Eds.), Methods of Soil Analysis: Part 4-Physical Methods.' Madison, WI: Soil Science Society of America, pp. 802-817.

Rhoades, J.D. (1996). Salinity: Electrical conductivity and total dissolved solids. In 'Sparks D.L. (Ed.), Methods of Soil Analysis: Part 3-Chemical Methods.' Madison, WI: Soil Science Society of America, pp. 417-435.

Ronsse, F., S. Van Hecke, D. Dickinson and W. Prins (2013). Production and characterization of slow pyrolysis biochar: Influence of feedstock type and pyrolysis conditions. GCB Bioenergy, 5 (2):104-115.

Shaaban, M., L. Zwieten, S. Bashir, A. Younas, A. Núñez-Delgado and M.A, Chhajro (2014). A concise review of biochar application to agricultural soils to improve soil conditions and fight pollution. Journal of Environmental Management, 232: 34-42.

Shendi, M.M., A.M. Abdallah and M.S. Gad (2024). Soil salinization processes in reclaimed lands of El-hammam, Egypt: Pedological and Geospatial Assessment. Journal of Arid Environments, 215: 104861.

Siengchum, T., N. Tippayawong and T. Wongsiriamnuay (2013). Production of bio-oil and biochar from municipal solid waste by slow pyrolysis. International Journal of Chemical Engineering and Applications, 4 (4): 225-229.

Singh, R., A. Mandal and K.K. Yadav (2022). Temperature-dependent physicochemical transformation of olive pomace biochar and its applications in pollutant removal: An insight into pore dynamics. Journal of Analytical and Applied Pyrolysis, 165: 105526.

Smith, K.M., J.M. Brannon, B.K. Northup and J.D. Hemming (2018). Olive pomace biochar: a study of physical structure and adsorption capacity. Journal of Cleaner Production, 190: 500-508.

Song, W. and M. Guo (2012). Quality variations of poultry litter biochar generated at different pyrolysis temperatures. Journal of Analytical and Applied Pyrolysis, 94: 138-145.

Sparks, D.L. (1996). Methods of Soil Analysis, Part 3: Chemical Methods. In 'Madison, WI: Soil Science Society of America and American Society of Agronomy'. Available online at: https://doi.org/10.2136/sssabookser5.3

Steiner, C., B. Glaser, W.G. Teixeira, J. Lehmann, W.E.H. Blum and W. Zech (2007). Nitrogen retention and plant uptake on a highly weathered central Amazonian Ferralsol amended with charcoal. Journal of Plant Nutrition and Soil Science, 170 (2): 282-289.

Suliman, W., J.B. Harsh and N.I. Abu-Lail, A.M. Fortuna, I. Dallmeyer and M. Garcia-Perez (2016). Influence of feedstock source and pyrolysis temperature on biochar bulk and surface properties. Biomass and Bioenergy, 84: 37-48.

Sumner, M.E. and W.P. Miller (1996). Cation Exchange Capacity and Exchange Coefficients. In 'Sparks D.L. (Ed.), Methods of Soil Analysis: Part 3: Chemical Methods Madison', WI: Soil Science Society of America, pp. 1201-1229.

Sun, K., B. Gao, K.S. Ro, J.M. Novak, Z. Wang, S. Herbert and B. Xing (2012). Assessment of herbicide sorption by biochars and organic matter associated with soil and sediment. Environmental Pollution, 163: 167-173.

Thipkhunthod, P., T. Ishikawa, N. Kobayashi and T. Minowa (2005). Effect of feedstock and operating conditions on nitrogen content in bio-oil from fast pyrolysis of poultry manure. Journal of the Japan Institute of Energy, 84 (8): 674-679.

Thomas, G.W. (1996). Soil pH and Soil Acidity. In 'Sparks D.L. (Ed.), Methods of Soil Analysis: Part 3-Chemical Methods Madison,' WI: Soil Science Society of America, pp. 475-490.

Tripathi, M., J.N. Sahu, J.N. and P. Ganesan (2016). Effect of process parameters on production of biochar from biomass waste through pyrolysis: A review. Renewable and Sustainable Energy Reviews, 55: 467-481.

Wang, Z., S. Bakshi, C. Li, S.J. Parikh, H.S. Hsieh and J.J. Pignatello (2020). Modification of pyrogenic carbons for phosphate sorption through binding of a cationic polymer. Journal of Colloid and Interface Science, 579: 258-268.

Wu, W., M. Yang, Q. Feng, K. McGrouther, H. Wang, H. Lu and Y. Chen (2021). Chemical characterization of rice straw-derived biochar for soil amendment. Biomass and Bioenergy, 47: 268-276.

Xu, G., O. Mašek and D. Crowley (2020). Poultry manure biochar: production, characteristics and effects on soil fertility and leaching. Waste Management, 105: 9-18.

Yin, Q., B. Zhang, R. Wang and Zhao, Z. (2017). Biochar as an adsorbent for inorganic nitrogen and phosphorus removal from water: A review. Environmental Science and Pollution Research, 24**:** 26297-26309.

Youssef, M.A., B. Ahmed and A.I. El-Shafie (2023). Pollution from organic waste in Egyptian agricultural zones: environmental impacts and mitigation. Environmental Monitoring and Assessment, 195: 205.

Yuan, J.H., R.K. Xu and H. Zhang (2011). The forms of alkalis in the biochar produced from crop residues at different temperatures. Bioresource Technology, 102 (3): 3488-3497.

Zaker, A., M. Dolatabadi, H. Hashemipour and K. Godini (2019). Optimization of biochar production from olive mill waste for nitrate removal: Influence of activating agents and pyrolysis temperature. Journal of Environmental Chemical Engineering, 7 (2): 102931.

Zama, E.F., K.C. Uzoma, Q.H. Zhu and Y.G. Zhu (2020). Animal manure biochar: A review on its production, properties and effects on soil and plant growth. Waste Management, 106: 146-160.

Zhang, J., Z. Chen, J. Liu, Z. Yu and Q. Lin (2020). A comprehensive review of thermal conversion of biomass: Pyrolysis, gasification, and liquefaction. Renewable and Sustainable Energy Reviews, 134: 110329.

Zhao, L., X. Cao, O. Mašek and A. Zimmerman (2013). Heterogeneity of biochar properties as a function of feedstock sources and production temperatures. Journal of Hazardous Materials, 256-257: 1-9.

Zhou, Y., B. Gao, A.R. Zimmerman, J. Fang, Y. Sun and X Cao (2015). Sorption of heavy metals on chitosan-modified biochars and its biological effects. Chemosphere, 136: 220-226.

تأثير نوع المادة الخام ودرجة حرارة التحلل الحراري على خصائص الفحم الحيوي والخصائص الفيزيائية والكيميائية للتربة في منطقة الحمام، مصر

سحر محمد إسماعيل
قسم كيمياء وفيزياء التربة، شعبة مصادر المياه والأراضي الصحراوية، مركز بحوث الصحراء، المطرية، القاهرة، مصر

في السنوات الأخيرة، ظهر الفحم الحيوي كإضافة مستدامة للتربة بهدف تحسين جودة التربة في المناطق الجافة وشبه الجافة التي تعاني من انخفاض الخصوبة ومحتوى المادة العضوية. إستهدفت هذه الدراسة إلى تقييم تأثير أنواع مختلفة من الفحم الحيوي الناتج من مخلفات زراعية محلية وهي تفل الزيتون (PO)، وروث الأغنام والماعز (GSD)، وسماد الدواجن (PM)، والتي تم تحللها الحراري عند درجات حرارة ٣٥٠، ٥٠٠ و٧٠٠ درجة مئوية على الخصائص الفيزيائية والكيميائية لتربة رملية متدهورة في منطقة الحمام، مصر. تمت عملية توصيف خصائص المواد الخام والفحم الحيوي الناتج باستخدام مجموعة من التحاليل المتقدمة، مثل تحليل proximate وتحليل ultimate، والتحليل الحراري الوزني والتحليل الحراري التفاضلي (TGA-DTA)، ومطياف الأشعة تحت الحمراء (FT-IR)، وتحليل مساحة السطح بطريقة (BET)، والميكروسكوب الإلكتروني الماسح (SEM)، وحيود الأشعة السينية (XRD)، (XRF). بناءً على الاستقرار البنائي ومساحة السطح ومحتوى العناصر الغذائية، تم اختيار الفحم الحيوي المنتج عند ٥٠٠ درجة مئوية لتنفيذ تجارب الأصص الزراعية داخل الصوبة الزجاجية، حيث تم تطبيق وتحضين كل نوع من الفحم الحيوي بنسب ٢ و٥٪ من وزن التربة (w/w) لمدة ٦٠ يومًا. تم تحليل خصائص الفحم الحيوي مثل درجة الحموضة (pH)، التوصيل الكهربائي (EC)، محتوى الرماد، التركيب العنصري والكثافة الحجمية. بعد انتهاء فترة التحضين، تم تقييم خصائص التربة مثل pH، EC، الكربون العضوي الكلي (TOC)، النيتروجين الكلي (TN)، نسبة الكربون إلى النيتروجين (C/N)، السعة التبادلية الكاتيونية (CEC)، المسامية، ومحتوى الماء المتاح (AWC). أظهرت النتائج أن نوع المادة الخام ودرجة حرارة التحلل الحراري كان لهما تأثير كبير على خصائص الفحم الحيوي واستجابة التربة. حيث حقق فحم تفل الزيتون عند ٥٪ و٥٠٠ درجة مئوية أعلى زيادة في الكربون الكلى بنسبة ٥٠٪ والمسامية بنسبة ٤٧,٩٢٪، وAWC بنسبة ١٤,٢٪. بينما أظهر فحم سماد الدواجن أعلى زيادة في CEC (٨٥ سنتى مول كج$^{-1}$)، في حين أعطى فحم روث الأغنام والماعز تحسينات متوسطة. بشكل عام، توصى هذه الدراسة بإستخدام فحم تفل الزيتون المنتج عند ٥٠٠ درجة مئوية وبمعدل تطبيق ٥٪ كأفضل تطبيق لتحسين خصوبة التربة واحتفاظها بالمياه في الظروف الجافة.